ACS NANO
Cite This: ACS Nano 2018, 12, 11552−11560
www.acsnano.org

ARTICLE

Assembly of Robust Holmium-Directed 2D Metal−Organic Coordination Complexes and Networks on the Ag(100) Surface

Martin Uphoff,[†,§] Georg S. Michelitsch,[‡,§] Raphael Hellwig,[†] Karsten Reuter,[‡] Harald Brune,[¶] Florian Klappenberger,[*,†] and Johannes V. Barth[*,†]

[†]Department of Physics (E20), Technische Universität München, James-Franck-Straße 1, 85748 Garching, Germany
[‡]Department of Chemistry, Chair of Theoretical Chemistry, Technische Universität München, Lichtenbergstraße 4, 85748 Garching, Germany
[¶]Institute of Physics, Ecole Polytechnique Fédérale de Lausanne (EPFL), Station 3, 1015 Lausanne, Switzerland

Supporting Information

ABSTRACT: We describe the formation of lanthanide−organic coordination networks and complexes under ultra-high-vacuum conditions on a clean Ag(100) surface. The structures comprise single Ho atoms as coordination centers and 1,4-benzenedicarboxylate (from terephtalic acid, TPA) as molecular linkers. Using low-temperature scanning tunneling microscopy, we find two different chiral phases of surface-supported metal−organic structures incorporating Ho atoms. Density functional theory calculations can explain the structure of both binding motifs and give possible reasons for their varying formation under the respective Ho/TPA ratios, as well as deposition and annealing temperatures. Metal−ligand interactions drive the formation of cloverleaf-shaped mononuclear Ho−TPA_4 complexes establishing supramolecular arrays stabilized through hydrogen bonding. A 2D lanthanide−organic reticulation is observed when changing the stoichiometry between the two building blocks. The combined insights from scanning tunneling microscopy and density functional theory reveal the relative stability, charge transfer, and bonding environment of both motifs.

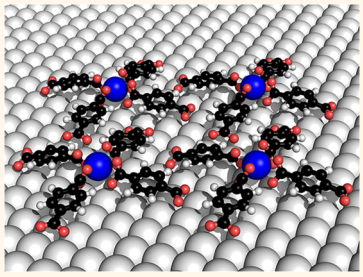

KEYWORDS: *metal−organic coordination, self-assembly, lanthanides, holmium, carboxylates, terephthalic acid, scanning tunneling microscopy, density functional theory*

In recent years the use of lanthanides in molecular architectures has been a burgeoning field of research, exploiting the high coordination numbers lanthanides offer in comparison to other metals. Inspired by the potential revealed in three-dimensional compounds and networks,[1−7] recent studies focus on the development and control of interfacial nanosystems[8−11] and architectures.[12−16] Additionally, their magnetic properties are of high interest to the scientific community, and major steps were done in the fabrication of lanthanide-based magnetic devices including single-molecule magnetic complexes.[17−23] Recent experiments reveal prospects toward single-atom memory for single Ho atoms on a surface.[24,25] They offer the ultimate smallest memory unit of magnetic storage devices, but are so far unstable in their confinement on the surface and exhibit loss of their magnetic hysteresis above 50 K.[26]

In order to stabilize single Ho atoms against diffusion on the surface, we utilize on-surface metal−organic self-assembly. As previously shown, the formation of coordination superlattices and networks permits creating and preserving stable magnetic quantum states, whereby the embedding of metal atoms in specific coordination configurations with organic ligands can greatly influence the electronic structure of the metal centers and hence their spin states.[20,21,23,27] Moreover, through changing the environment by such measures, the lifetime of the spin states can be greatly increased.[28]

In this work, we explore the potential of organic linker molecules combined with Ho atoms at a well-defined metal surface toward the formation of robust metal−organic nanostructures. We employ a simple, prototypical linker species, namely, 1,4-benzenedicarboxylic acid (terephtalic acid - TPA). It is a versatile building block for the creation of supramolecular architectures on noble metal surfaces and semiconductors[29−31] and has also been employed for lanthanide-based metal−organic coordination.[32] On reactive surfaces, thermal excitation can transform the functional groups into carboxylate species whereby the deprotonation can drive phase transformations[33] and enable the formation of metal−organic coordination motifs.[28] Utilizing scanning

Received: September 2, 2018
Accepted: October 8, 2018
Published: October 8, 2018

DOI: 10.1021/acsnano.8b06704
ACS Nano 2018, 12, 11552−11560

tunneling microscopy (STM), we investigate the self-assembly behavior on Ag(100), *i.e.*, a weakly reactive surface with square symmetry. Although there is a relatively high activation barrier for deprotonation on this substrate, it was chosen because it provides the possibility to afford magnesium oxide layers, thus creating interfaces with exceptional properties regarding lanthanide-based nanomagnetism.[24,34]

Through first characterizing purely organic adlayers we show that heating-induced deprotonation generates a carboxylate precursor phase before significant loss of molecules through desorption sets in. This enables the subsequent creation of Ho-directed nanostructures. *Via* controlling the preparation conditions (*i.e.*, Ho-molecule ratio, deposition, and annealing temperatures), we can steer the formation of two distinct Ho–TPA phases consisting of metal–organic complexes and coordination networks, respectively. By means of density functional theory (DFT) calculations we develop structural models for the supramolecular assemblies explaining the experimental findings in great detail. Furthermore, through the DFT analysis we gain insight into the Ho coordination chemistry including the charge redistribution of the coordination nodes and the influence of the surface. We give an explanation for the chirality of the structures and a detailed analysis of strain effects, which are of general relevance in the field of surface-confined metallosupramolecular engineering. Our work highlights the potential of Ho for the construction of surface-supported large-scale nanoarchitectures that bear prospects for nanomagnetism. Simultaneously, we lay a foundation to further exploit the exceptional magnetic properties of Ho on surfaces that arise from the occurrence as single confined entities.

RESULTS AND DISCUSSION

Before we investigated Ho-directed structure formation we characterized samples with purely organic adlayers aiming at the preparation of a reactive precursor layer featuring functional groups in the carboxylate state, thus ready to coordinate to lanthanide atoms. In a first attempt, TPA molecules were deposited onto a freshly cleaned Ag(100) surface held at room temperature *via* organic molecular beam epitaxy (OMBE, T_{OMBE} = 160 °C).

The preparation resulted in long-range ordered domains where all molecules exhibited the same apparent height (Figure 1a, inset, note that all presented STM images were recorded at 4.5 K). The intermolecular distance along the molecular chains, d_0 = 9.7 Å, is consistent with previous reports on hydrogen-bonded assemblies of intact TPA, as suggested by the superimposed molecular models. Subsequent annealing of the sample resulted in strong desorption losses, disqualifying this approach as a starting point for Ho-carboxylate architectures. The comparison to previous results on Cu(100)[28,35−37] and Ag(111)[38] indicates that the adhesion of TPA to the Ag(100) surface is quite limited and more similar to the close-packed Ag(111) than to the Cu(100).

Then, we developed a so-called hot deposition approach, where TPA is deposited onto a hot substrate; that is, the sample is held at 450 K during the 10 min deposition time. STM data obtained on that sample reveal that this preparation protocol results in a purely organic phase with a coverage near to one monolayer (ML). The molecules form a regular adsorption pattern (Figure 1a), in which they appear as oval protrusions exhibiting either one of two relative brightness levels. A brighter species is surrounded by six darker ones,

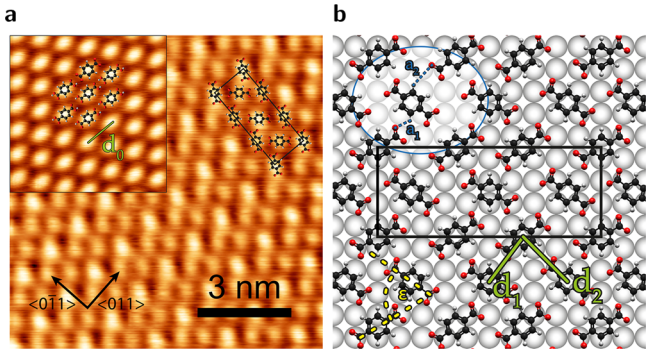

Figure 1. Precursor phase (a) STM image of an organic layer consisting of TPA molecules with deprotonated end groups on the Ag(100) surface obtained upon adsorption at 450 K. A regular pattern of molecules appearing to be higher in topography is visible, Inset: TPA deposited at RT on Ag(100). Tunneling current I_T = 1.1 nA, bias voltage V_B = 3 mV. (b) Tentative model of the organic precursor layer. The heterogeneous topography distribution of the molecules is due to higher lying TPA molecules on the bridge sites of the silver substrate. The unit cell of the organic network is marked as a black rectangle, identifying it as a $p(10 \times 4)$ structure with respect to the underlying lattice.

while each darker species is surrounded by three brighter and three darker ones. Thus, the unit cell outlined in the figure now contains six molecules. The prominent differences regarding relative brightness, unit cell size, and orientation of the molecules in comparison to the previous phase of intact TPA (Figure 1a, inset) indicate that the adsorbates should now exhibit a different substrate registry and chemical nature.

The small overlay in the top right corner of Figure 1a depicts the orientation of the molecules, and a tentative adsorption model is presented in Figure 1b. Following previous NEXAFS studies of TPA on Cu(100),[33] we assume a flat adsorption geometry of the phenyl ring on the surface. The model describes the adlayer as a $p(10 \times 4)$ superstructure with a density of 0.15 molecule per Ag atom and consists of doubly deprotonated TPA, *i.e.*, where both functional groups are in the carboxylate state and the phenyl ring still contains its four H atoms. It rationalizes the relative brightness pattern through associating the dimmer and brighter species with molecules adsorbed with their phenyl ring centered on hollow and bridge sites of the Ag lattice, respectively. Additionally, the model shows a slight rotation of the hollow site molecules around the normal vector of the phenyl ring plane. This results in a distorted T-shaped binding motif, where the carboxylates do not face the hydrogen atoms of the phenyl rings in an exactly perpendicular fashion, but rather at an angle of ε = 73°, as depicted in Figure 1b. We suggest that the center positions of the molecules are determined by molecule–substrate interaction, whereas weak, noncovalent lateral interactions between the molecules, presumably dominated by proton acceptor ring interaction,[39] induce the rotation of the molecules. The occurring intermolecular distances of nearby atoms are situated between a minimum of a_1 = 2.1 Å and a maximum of a_2 = 3.5 Å (blue circle in Figure 1b), thus exhibiting typical values for noncovalent interaction.[40]

By a detailed analysis of the distances between molecules, we obtain indirect evidence on their chemical state. The two nearest neighbor distances of the precursor phase are labeled as d_1 and d_2 in Figure 1b. Considering the substrate registry, the distances between bridge and hollow site molecules (d_1) are

DOI: 10.1021/acsnano.8b06704
ACS Nano 2018, 12, 11552–11560

7.2 Å and between two hollow site molecules (d_2) 8.2 Å, respectively. The layer is denser than the previous assembly of intact TPA (*cf.* Figure 1a inset), where the corresponding distances amount to 7.2 and 9.7 Å (d_0). Previous studies revealed consistent values. Assemblies of doubly deprotonated TPA on Cu(100) exhibited $d_1 = d_2 = 7.65$ Å.[36] Similar distances ($d_1 = d_2 = 7.4$ Å) were also found on Pd(111).[41] By contrast, packing schemes of intact TPA on Au(111)[42] showed $d_1 = 8.5$ Å and $d_2 = 9.9$ Å, consistent with our values for the intact phase and with the case of intact TPA on Cu(100), where $d_1 = 8.1$ Å and $d_2 = 12.8$ Å.[33] This comparison strongly indicates that the precursor phase on Ag(100) contains predominantly doubly deprotonated TPA.

We thus conclude that the described hot deposition method enables us to obtain a full ML of ditopic carboxylate linkers with very few impurities and defects. This is a favorable outcome, since later annealing steps for the preparation of metal−organic coordination networks (MOCNs) always result in a slight loss of molecules due to thermal desorption.

For coverages below a full ML (again obtained by hot deposition) two organic phases are present. Besides the precursor phase discussed above, small islands of a less dense phase form between the big islands of the precursor phase. Details on this "transition phase" are given in the Supporting Information (*cf.* S1(a)).

Ho-Directed Assembly. For investigating the potential of surface-supported Ho as coordination centers we prepared a series of samples systematically varying the preparation parameters. We obtained the best results for dosing Ho at room temperature onto a full monolayer of the precursor phase followed by annealing the sample at 450 K for 10 min. Depending on the Ho dosage, two different types of metal−organic structures were observed. Ho dosages refer to fractions of monolayers of the close-packed Ho(0001) surface (hcp crystal lattice, see Supporting Information).

Cloverleaf Phase. An STM image of a TPA/Ag(100)-$p(10 \times 4)$ precursor sample exposed to a low dosage of Ho (~0.015 ML) is depicted in Figure 2a.

The essential binding motif is composed of four bright features pointing toward a medium bright center interpreted as a cloverleaf shape (red outline). Similar cloverleaf phases have been reported on Cu(100), involving iron or gadolinium[15] as coordination centers and multitopic carboxylate linkers[43,44] including TPA.[36] Analogously, we suggest that here four linker species coordinate to one Ho atom, as depicted by the model overlay, making it an 8-fold coordination to the surrounding oxygens. According to STM data, the unit cell vectors of this metal−organic superstructure enclose an angle of 22.2 ± 1.8° with respect to the primitive lattice vectors of the Ag(100) surface (shown in the bottom left corner of Figure 2a). This corresponds to a quadratic unit cell of 15.6 ± 0.08 Å.

With our DFT-based geometry optimization we obtained the adsorption model shown in Figure 2b, where the unit cell is highlighted by a black rectangle. It confirms that four carboxyl groups are coordinated to one Ho atom. More specifically, the involved carboxylates are concertedly rotated by an angle of 53° around the C−C axis connecting them to the phenyl rings, thus rendering a chiral coordination scheme. This behavior of the linker groups was weakly implied in a previous study[15] and can now be confirmed by our calculations. The chirality is better visualized in Figure 4a and b, depicting the two enantiomers side-by-side. It has been shown that the adsorption of achiral molecules can entail surface-induced

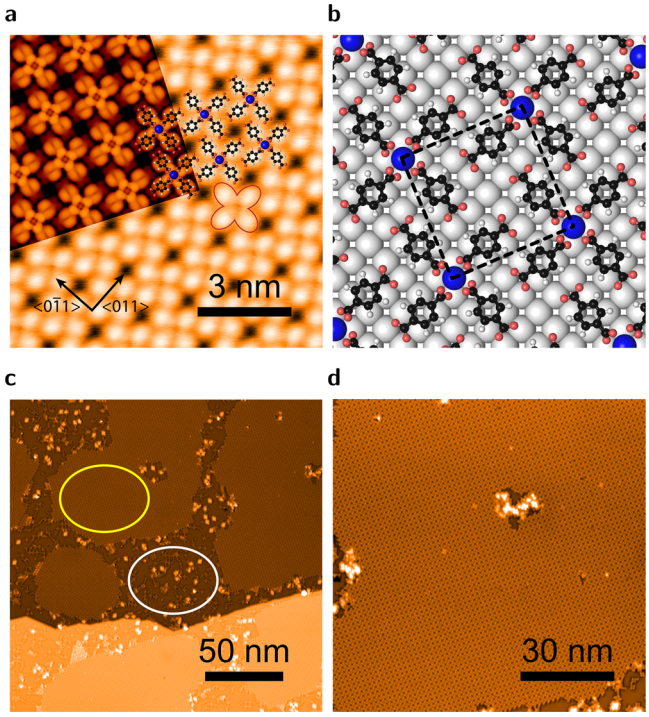

Figure 2. (a) High-resolution constant-current STM image of the Ho(TPA)$_4$/Ag(100)-$p(\sqrt{29} \times \sqrt{29})R21.8°$ cloverleaf phase, superimposed by a simulated STM image rendered from the DFT model. Molecules and Ho atoms are superimposed to mark their positions (I_T = 500 pA, V_B = −2 mV). (b) DFT model for the cloverleaf phase. The unit cell is marked by the dashed square. (c) 200 nm × 200 nm STM image showing the extent of islands on the silver surface. There are some clusters and molecules in the organic transition phase present, partly decorated by Ho adatoms (example area indicated by white ellipsoid). (d) 100 nm × 100 nm excerpt from (c) showing the quality of the islands.

chirality along with chiral recognition on the formation of extended islands, greatly influencing the electronic structure.[45] This could be utilized to steer the systems nanomagnetic properties. The arrangement of the metal−organic complexes is forming a fully commensurate pattern. The top-left part of Figure 2a depicts an overlay of a simulated STM image calculated from the model and demonstrates the excellent agreement with the observed features in the STM data.

In our DFT calculations Ho atoms preferentially reside at the energetically favorable[46] hollow positions of the silver lattice and the lower O atoms of the carboxylates assume positions close to the Ag top sites. With respect to the primitive crystal directions the unit cell constitutes a square $p(\sqrt{29} \times \sqrt{29})R21.8°$ superstructure with a size of 15.56 Å × 15.56 Å, agreeing nicely with the experimental value of 15.6 Å for the side length. The molecule density is 0.14 molecule per silver atom. Moreover, the cloverleaf phase exhibits organizational chirality, and both enantiomorphic arrangements have been observed on the same sample (see Supporting Information Figure S2).

The TPA molecules appear as bright oval protrusions in the STM image, whereas the Ho atoms appear transparent. The fact that the metal centers are not producing visible features in STM data is commonly observed for metal−organic coordination motifs.[15,47,48] Through translating the theoretical model with respect to the STM data, it can be inferred that the

DOI: 10.1021/acsnano.8b06704
ACS Nano 2018, 12, 11552−11560

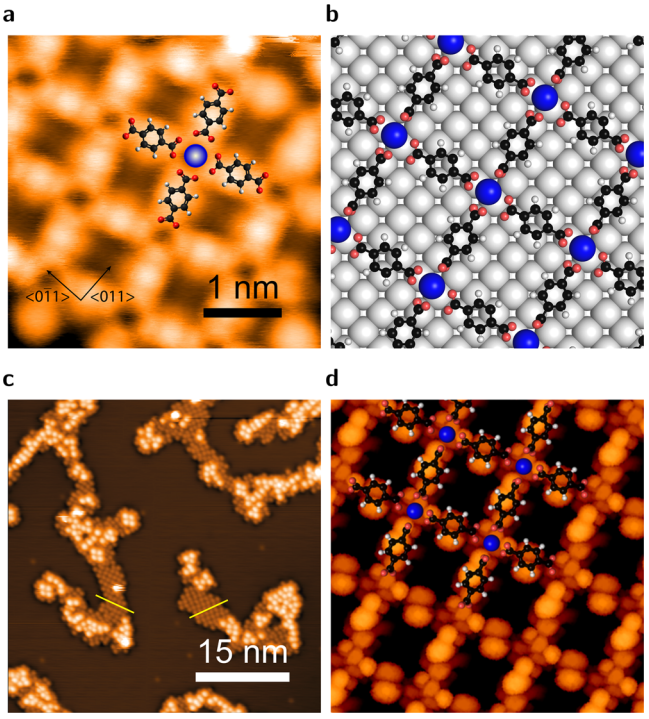

Figure 3. (a) High-resolution constant-current STM image of the Ho(TPA)$_2$/Ag(100)-$p(\sqrt{17} \times \sqrt{17})R14.04^\circ$ checkerboard phase. Molecules and Ho atoms are superimposed to mark their positions. (b) DFT model for the checkerboard phase. (c) 200 nm × 200 nm STM image showing the extent of islands on the silver surface. The islands are rather small and decorated on the edges by excess Ho atoms. The yellow lines indicate the two domain orientations. (d) Simulated STM signature of the checkerboard structure.

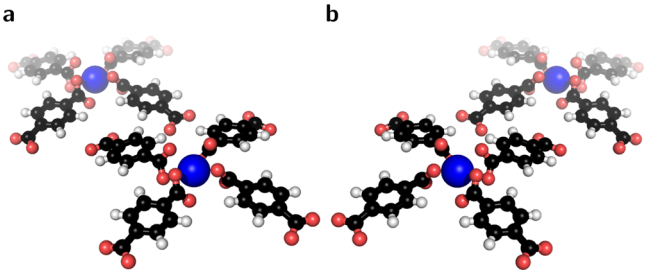

Figure 4. (a, b) Bonding environment in the mononuclear cloverleaf structure with the carboxylate linkers tilted by approximately 53° with respect to the molecular plane. As can be seen, the complex is chiral due to the concerted rotation of the carboxyl groups.

linkers reside with their phenyl rings on the hollow site of the Ag(100) surface and their long axis parallel to the ⟨011⟩ directions. This positioning is equivalent to that of TPA coordinated by Fe on Cu(100).[28] Assuming the hollow site for the phenyl ring is in accordance with previous findings of aromatic molecules on metal surfaces.[49−52] We substantiate this with our DFT calculations, as shown in Figure 2b.

The Ho atoms in the cloverleaf phase are 8-fold coordinated to the carboxylate ligands. This is a key difference with respect to the cloverleaf phase of TPA-Fe on Cu(100), where the iron is 4-fold coordinated. We assign this behavior to the rather ionic character of lanthanide−organic compounds featuring higher coordination numbers[53] and the increased surface area available for coordination in the case of Ho with significantly larger atomic diameter as compared to iron. A similar 8-fold coordination motif was reported for Gd atoms and TPA on Cu(111).[15] The rare earth atoms do not differ significantly in their chemical properties since the 4f-shell is located below the 6s^2 orbitals. The TPA molecules face the Ho atoms with one of their carboxylate groups, which must rotate out of the substrate plane for steric reasons. Studies of Dy-TPA architectures not involving DFT calculations were presented in terms of a coplanar orientation of the carboxylates.[32] However, our DFT calculations clearly reveal a concerted rotation of the functional groups in those structures, in agreement with Urgel *et al.*[15] DFT simulations of the proposed bonding model (more details for DFT calculations given below) yield a Ho−O distance of 2.3−2.4 Å and a Ho−C distance of 2.7 Å. These distances are in accordance with previous findings for gadolinium−carboxylate molecular assemblies, where the Gd−O distance was found to be 2.6 and 2.4−2.7 Å, as deduced from the experimental analysis and DFT calculations, respectively.[15]

As mentioned above, we propose an adsorption of the molecules at the hollow positions of the silver lattice and along the ⟨011⟩ directions. This results in a distance of 3.0−3.2 Å between the oxygen atoms of the uncoordinated carboxylate group and the hydrogen atoms of the molecule facing each other in a T-shape fashion. This distance suggests comparably weak lateral bonding. Thus, molecule−substrate interaction should dominate the forces on the uncoordinated functional group. Consistently, our DFT calculations demonstrate that the uncoordinated carboxylate groups act as anchors to the surface, as evident from the charge transfer analysis below.

More interesting are the possibilities for binding between neighboring molecules arranged next to each other in the same orientation and slightly shifted along their axis. Here, two hydrogen atoms are very close to each other (2.1 Å) and cause a repulsive force between the molecules. On the other hand, one of the free carboxylate oxygen atoms is close to one of the ortho-hydrogen atoms, and their distance of 3.0 Å would result in an attractive force caused by hydrogen bonding. These effects seem to balance each other out, leading to a configuration of the molecules as described above. Nonetheless, a slight shift and turn of the molecules would be compatible with our STM observations and would increase the H−H distance. In fact, the DFT calculations show a slight shift of the phenyl ring away from the hollow position, and thereby the H−H distance is increased to 2.2 Å.

When examining islands on a larger scale, we observed that the cloverleaf phase forms extended regular domains up to 200 nm in diameter. The limitation is presumably imposed by the size of the substrate terraces. Figure 2c depicts an overview image of a typical sample with an island of the cloverleaf phase highlighted by the yellow ellipsoid. We were able to get up to ∼70% of the silver surface covered with the cloverleaf phase. This filling factor refers to the area fraction of the substrate covered with the cloverleaf phase, determined by STM topography images and averaged over several frames. Although the molecule density is lower than in the precursor phase, it was not possible to obtain a saturated monolayer. We associate this behavior with the desorption of molecules during the annealing step. The islands show a high regularity and nearly no defects. This indicates an effective self-correcting mechanism during the assembly of the metal−organic structure. Also after annealing the sample again to 450 K the islands persist and no significant desorption took place.

DOI: 10.1021/acsnano.8b06704
ACS Nano 2018, 12, 11552−11560

However, since all measurements were done at low temperatures, it is not possible to determine whether the islands are stable up to that temperature or whether they dissolve and reform upon cooldown. The rest of the surface is bare silver or covered by a small amount of molecules (~2.5% of the entire surface), partly decorated by Ho clusters. In Figure 2c, the white ellipsoid indicates an area of the surface where these molecules can be seen. The molecules not participating in the cloverleaf phase are arranged in the purely organic transition phase described in the Supporting Information (darker protrusions in the white ellipsoid in Figure 2c). Some of these molecules have a Ho adatom adsorbed on their center (bright protrusions), presumably on the phenyl ring. Upon higher Ho dosage all additional molecules can be incoporated in Ho–adatom complexes, mostly consisting of four TPA molecules in a quadratic arrangement with four Ho atoms on top.

Checkerboard Phase. Increasing the Ho dosage applied to a precursor sample by a factor of 10 (~0.15 ML) leads to the formation of a different metal–organic phase. An exemplary STM image is shown in Figure 3a. The TPA molecules now interlink Ho centers, making the phase a MOCN, which we henceforth call checkerboard phase. Opposing molecules adsorb collinearly and exhibit uniform contrast, so an 8-fold coordination is present, with all oxygen atoms orientated toward the Ho atoms. This results in a stoichiometry of 1:2 of Ho:TPA. The close-up STM topography in Figure 3a clearly resolves the orientation of the molecules, as indicated by the overlaid TPA models. The phenyl ring appears as a round protrusion in the middle of two oval protrusions marking the positions of the carboxylate groups. Again, the Ho atoms do not produce visible features in STM, for the same reasons as discussed above for the cloverleaf phase. However, the positioning of the molecules can only be reconciled by the presence of Ho coordination centers.

A model of the checkerboard phase is reproduced in Figure 3b. Similar to the cloverleaf phase, the vectors of the unit cell are rotated with respect to those of the substrate. An analysis of the model reveals a $p(\sqrt{17} \times \sqrt{17})R14.04^{\circ}$ superstructure with a local molecule density of 0.12 molecule per silver atom. Its domains can be rotated both clockwise and counterclockwise with respect to the silver substrate. The end groups of the carboxylates are concertedly rotated in both network directions, similar to the cloverleaf phase, as evident from the DFT calculations. The latter also reveal that for Ho at hollow positions appreciable strain exists, which is understood as the reason that the Ho atoms are now moved to bridge sites. Also, the phenyl rings of the TPA molecules reside on the bridge positions of the Ag(100) surface. Figure 3c shows the expected two enantiomorphic structures in the bottom part of the image, where the two domain orientations are indicated by yellow lines.

It can also be seen in the figure that the island size is very small (strips of ~5 nm width) compared to the cloverleaf phase. A possible explanation is that due to the larger unit cell the silver substrate enforces upon the MOCN, the bond formation capability with the interconnecting nodes is impaired. This hypothesis is strongly corroborated by the DFT simulation as discussed later. We were not able to obtain coverages beyond approximately 15% of the surface with this phase, although we started off with a full monolayer of the precursor phase. The small islands always come with additional Ho atoms adsorbed on some of the molecules and show an anisotropic, ribbon-like growth. Again, the networks remain after reheating the sample to 450 K and subsequent cooldown.

A simulated STM image is shown in Figure 3d. The anisotropic differences in contrast could not be resolved *via* STM, probably due to unknown tip effects at such low bias voltages.

It has to be noted here that although the Ho dosage on the surface is 10 times higher than with the cloverleaf phase, the amount of anticipated Ho on the surface inferred from STM data (*cf.* Figure 3c) does not match the preparation stoichiometry. We propose a higher desorption of Ho–carboxylate complexes and clusters with Ho acting as an enhancing agent in the mechanism, although this is just a hypothesis and we cannot support this by other experiments or calculations. Decoration of step edges could also interfere.

DFT Analysis of Ho–TPA Networks. Dispersion-corrected DFT calculations were performed for periodic supercells of both structures. A free-standing overlayer of the checkerboard phase was allowed to freely adsorb on the metal slab to find the equilibrium adsorption geometry. This approach is similar to previous calculations on metal–carboxylate architectures on metal surfaces.[47,S4] The calculations reveal a severe strain of the checkerboard structure, when stacked commensurably onto the Ag(100) surface. The silver lattice then imposes a Ho–Ho distance of 11.9 Å on the entire structure, while a free-standing layer of the structure would have a lattice periodicity of 11.4 Å. If the initial C_4-symmetric geometry with the Ho atom centered on the Ag(100)-hollow site is optimized toward an equilibrium structure, the geometry relaxation will always break the linker–Ho bond on one end of the TPA molecule (*cf.* Figures 4 and S4 in the Supporting Information). Figure 5 shows an intermediate 8-fold-coordinated MOCN structure with the Ho atom adsorbed on the hollow site and the directions of the forces acting on the respective atoms. The structure does not represent a global minimum of the potential energy surface, and the forces acting on the molecule would require to break open one or both carboxyl–Ho bonds to relieve the strain.

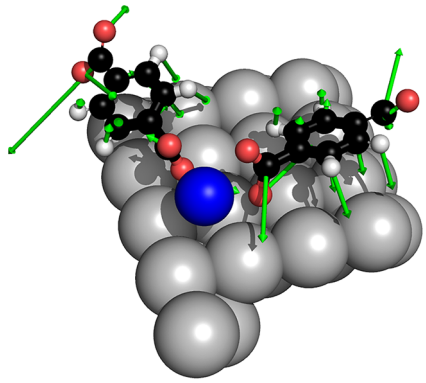

Figure 5. Forces (green vectors) acting on the linker molecules in the unrelaxed checkerboard structure where the Ho is still positioned in the hollow place (*cf.* Figure S4, H2). Magnitude of vectors not to scale.

A fully reticulated two-dimensional metal–organic framework could only be stabilized by allowing this symmetry breaking from the initially assumed C_4 to a C_2 symmetry axis centered on the Ho atom. The reduction in symmetry is

DOI: 10.1021/acsnano.8b06704
ACS Nano 2018, 12, 11552–11560

Table 1. Mulliken Charges of the Cloverleaf and Checkerboard Structures per Atom and per Unit Cell[a]

	cloverleaf				checkerboard		
charge	O^{surf}	O^{Ho}	Ho	Ag	O	Ho	Ag
e/atom	−0.32	−0.37	+1.17	+0.05	−0.36	+1.12	+0.01
e/cell	−2.54	−2.95	+1.17	+1.47	−2.90	+1.12	+0.46

[a]In the cloverleaf structure, two distinct species of oxygen atoms are present, the Ho-bonded O^{Ho} and the surface-anchored O^{surf}.

accompanied by the Ho atom leaving the Ag(100) hollow sites. This removes part of the strain in the structure, since the TPA molecule does not need to bend from one hollow site toward the next one. We assign this observed strain as the primary reason that the checkerboard pattern could only be observed in small band-shaped islands of less than 10 observable subunits in the shorter dimension, as opposed to MOCNs with commensurable registry.[12,36,48] A symmetry reduction is also discernible in the STM data, in the shape of the framework hollow sites, where either cushion-shaped C_4-, C_2-, or C_1-symmetric squares with concave arched edges are observed. This symmetry breaking due to substrate-induced stress is also reflected in the simulation. A Mulliken population analysis (as listed in Table 1 for Ho, Ag, and O) suggests charge transfer from the Ho atom toward the carboxylate linker atoms. Further electron density is depleted from the surface in the vicinity of the bonding node (*cf.* Figure 6).

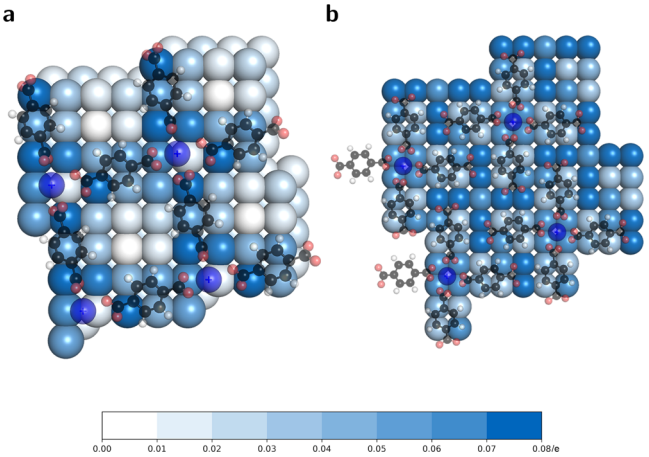

Figure 6. Hotspots of the charge transfer between the substrate and the adsorbate. Highlighted in blue are the areas of high electron depletion compared to white (no electron charge depletion) in fractions of *e*. Adsorbate shown without color coding for reference purposes.

The C_4-symmetric arrangement of the cloverleaf deduced from the experimental data is fully consistent with our calculations. The optimized geometries obtained for both the high-symmetry cloverleaf and the broken-symmetry checkerboard phase are stable minima of the potential energy surface with relaxed bond distances fully consistent with those derived from the STM measurements, thereby strongly supporting the structural models derived from the experimental data. The simulated STM images in Figures 2a and 3d indicate that the Ho site is transparent at the employed tunneling conditions, since the 4f eigenstates in both bonding environments lie at far too high and low energies with respect to E_F. Indeed, there is a local minimum seen at the interconnecting Ho nodes in the experimental data. Similar observations for different lanthanide atoms have already been reported elsewhere.[15] The smaller, yet bright protrusions around the central depression (Ho center) are clearly unoccupied states of the neighboring carboxylic oxygens, in our simulations presumably overdelocalized by the employed semilocal DFT functional.[55] To a much smaller extent the same signatures are also visible in some of the experimentally recorded images as shown in Figures 2a and 3a. The Mulliken population analysis shown in Table 1 for Ho, Ag, and two species of nonequivalent oxygen atoms suggests very similar values for the charge transfer from both the Ho and the substrate toward the carboxylate linkers. The charge transfer from the substrate occurs primarily at two points: the anchor points of the dangling carboxylate linkers and at the Ho node (*cf.* Figure 6). In contrast to the cloverleaf structure, all carboxylate groups in the checkerboard pattern are rotated out of plane to accommodate the bonding environment and effectively reduce the charge transfer. The charges do not add up to zero, because only atoms with charge transfer to the surface are listed here.

CONCLUSIONS

In conclusion, two different types of thermally robust molecular architectures of TPA and Ho on the Ag(100) surface were fabricated by finely tuning the deposition parameters. We were able to build up enantiomorphic islands of mononuclear lanthanide−carboxylate compounds with $Ho(TPA)_4/Ag(100)$-$p(\sqrt{29} \times \sqrt{29})R21.8°$ structure, high lateral extent, surface coverage, and low defect density. Reticulated MOCNs have a $Ho(TPA)_2/Ag(100)$-$p(\sqrt{17} \times \sqrt{17})R14.04°$ structure and feature reduced island sizes due to interfacial strain effects. The two observed metal−organic architectures are both chiral, due to a rotation of the superstructure with respect to the silver lattice and a concerted rotation of the carboxylates. In the case of the cloverleaf phase conformational chirality is also present. These structural models receive further support by DFT calculations, which identified high strain as a potential reason for the limited extent to which the checkerboard phase could be grown experimentally. The chiral signature of the Ho coordination sphere could afford intriguing new magnetic features. Additionally, our DFT calculations give insight into the charge redistribution within the molecular architectures. Stabilization of single Ho atoms with 8-fold coordination in the cloverleaf structure is a particularly promising approach to exploit the recently found magnetic properties of Ho atoms on surfaces without being hampered by the onset of Ho diffusion at low temperatures. This work shows that Ho can be stably deployed as single atoms on surfaces, which opens up the possibility to investigate the nanomagnetic properties of Ho in a well-defined molecular environment, *e.g.*, by means of X-ray magnetic circular dichroism. The possibility to grow insulating decoupling layers such as NaCl or MgO on Ag(100) provides prospects to tune their magnetic properties *via* supramolecular on-surface engineering, and a comparison of Ho−carboxylates on both MgO and Ag will give further insight into this intriguing field of research.

METHODS

Experimental Details. Measurements were performed under ultra-high-vacuum conditions (base pressure below 2.0×10^{-11} mbar) with a commercial Joule-Thomson-STM from SPECS. For this work

DOI: 10.1021/acsnano.8b06704
ACS Nano 2018, 12, 11552−11560

experiments were carried out at 4.5 K. All shown images were taken in constant current mode using electrochemically etched tungsten tips that were cleaned by Ar-ion sputtering and field emission on a clean silver surface. The bias voltage was applied to the sample.

Samples were prepared by repeated cycles of Ar-ion (U = 0.9 kV) sputtering and annealing at 500 °C. We used a Ag(100) crystal from Surface Preparation Laboratory. The TPA molecules were purchased from Fluka (purity ≥99%) and evaporated from a home-built quartz crucible Knudsen cell at a temperature of 160 °C. Prior to preparation the molecules were degassed for purification extensively. The Ho atoms were evaporated *via* a home-built foil evaporator (see Supporting Information). The sample temperatures were measured *via* a thermocouple directly on the crystal.

Computational Details. Dispersion-corrected DFT calculations were performed for periodic supercells with the FHI-aims[56] computing package. Geometry optimizations for the smallest possible surface unit cell comprising two (four for cloverleaf) TPA molecules and one atom of Ho were performed with FHI-aims at "tight" computational settings ("light" for Ag), 3 × 3 × 1 k-point sampling, and using a 30 Å vacuum region. In these calculations electronic exchange and correlation was treated on the generalized-gradient approximation level with the PBE[55] functional, augmented by dispersive interactions through the Tkatchenko–Scheffler TS^{surf} method.[57] In order to improve the description of the strong local coulomb interaction of the 4f electrons, a Hubbard-type correction (DFT+U) was employed. The value of U = 5.8 eV for the Ho 4f states was chosen to reproduce the energetic splitting of occupied and unoccupied states of a model Ho[OAc]$_3$ complex treated on the HSE06[58] level (details given in the Supporting Information). The metal–organic compound was fully relaxed until residual forces were below 2.5 × 10^{-3} eV/Å. The cell size was chosen to match integer multiples of the optimal lattice constant for bulk silver as obtained by a fit to the Birch–Murnaghan equation of state. The experimental results suggest a $\sqrt{17} \times \sqrt{17}R14.0°$ conformation for the checkerboard pattern and a $\sqrt{29} \times \sqrt{29}R21.8°$ conformation for the cloverleaf pattern. The Ho–Ho distance thus determines the repetition unit, and the required metal surface unit cell was adapted to form a closed surface (4 × 4 for checkerboard and 5 × 5 for cloverleaf, respectively). In the geometry optimizations of the checkerboard structure the first metal slab layer was allowed to relax. For the larger cloverleaf pattern only one fixed layer of Ag was used to mimic a metal support. For the optimized geometries, the Tersoff–Hamann approach[59] was employed to simulate STM images, providing a means of directly comparing the electronic structure of the obtained geometry to the experimental signature. Integration over all electronic density of states within 20 meV around the metallic Fermi level produced the final image. The obtained images were smoothened using the rolling ball algorithm[60] with a ball radius of 0.5 Å.

ASSOCIATED CONTENT

Supporting Information

The Supporting Information is available free of charge on the ACS Publications website at DOI: 10.1021/acsnano.8b06704.

> Organic transition phase, chirality of Ho–TPA$_4$ complexes, determination of the U-value, structural relaxation details, node bonding environment, experimental details (PDF)

AUTHOR INFORMATION

Corresponding Authors

*E-mail: florian.klappenberger@tum.de.
*E-mail: jvb@tum.de.

ORCID

Martin Uphoff: 0000-0003-3480-4632
Georg S. Michelitsch: 0000-0003-2392-9413
Karsten Reuter: 0000-0001-8473-8659
Harald Brune: 0000-0003-4459-3111
Florian Klappenberger: 0000-0002-2877-6105
Johannes V. Barth: 0000-0002-6270-2150

Author Contributions

§M. Uphoff and G. S. Michelitsch contributed equally to this work.

Notes

The authors declare no competing financial interest.

ACKNOWLEDGMENTS

This work has been funded by the German Excellence Initiative and the European Union Seventh Framework Programme, under support of the Technische Universität München and its Institute for Advanced Study under grant agreement no. 291763. Funding was also provided by the ERC Advanced Grant MolArt (grant no. 247299) and the German Research Foundation via KL 2294/6-1 and is gratefully acknowledged. G.S.M. and K.R. gratefully acknowledge the Gauss Centre for Supercomputing e.V. (www.gauss-centre.eu) for funding this project by providing computing time on the GCS Supercomputer SuperMUC at Leibniz Supercomputing Centre (www.lrz.de) under grant no. PR92ME.

REFERENCES

(1) Bünzli, J.-C. G. Review: Lanthanide Coordination Chemistry: From Old Concepts to Coordination Polymers. *J. Coord. Chem.* **2014**, *67*, 3706–3733.

(2) Reineke, T. M.; Eddaoudi, M.; Fehr, M.; Kelley, D.; Yaghi, O. M. From Condensed Lanthanide Coordination Solids to Microporous Frameworks Having Accessible Metal Sites. *J. Am. Chem. Soc.* **1999**, *121*, 1651–1657.

(3) Pan, L.; Adams, K. M.; Hernandez, H. E.; Wang, X.; Zheng, C.; Hattori, Y.; Kaneko, K. Porous Lanthanide-Organic Frameworks: Synthesis, Characterization, and Unprecedented Gas Adsorption Properties. *J. Am. Chem. Soc.* **2003**, *125*, 3062–3067.

(4) Qin, C.; Wang, X.-L.; Wang, E.-B.; Su, Z.-M. A Series of Three-Dimensional Lanthanide Coordination Polymers with Rutile and Unprecedented Rutile-Related Topologies. *Inorg. Chem.* **2005**, *44*, 7122–7129.

(5) Long, D.-L.; Blake, A. J.; Champness, N. R.; Wilson, C.; Schröder, M. Lanthanum Coordination Networks Based on Unusual Five-Connected Topologies. *J. Am. Chem. Soc.* **2001**, *123*, 3401–3402.

(6) Long, D.-L.; Hill, R. J.; Blake, A. J.; Champness, N. R.; Hubberstey, P.; Proserpio, D. M.; Wilson, C.; Schröder, M. Non-Natural Eight-Connected Solid-State Materials: A New Coordination Chemistry. *Angew. Chem., Int. Ed.* **2004**, *43*, 1851–1854.

(7) Long, D.-L.; Blake, A. J.; Champness, N. R.; Wilson, C.; Schröder, M. Unprecedented Seven- and Eight-Connected Lanthanide Coordination Networks. *Angew. Chem., Int. Ed.* **2001**, *40*, 2443–2447.

(8) Écija, D.; Auwärter, W.; Vijayaraghavan, S.; Seufert, K.; Bischoff, F.; Tashiro, K.; Barth, J. V. Assembly and Manipulation of Rotatable Cerium Porphyrinato Sandwich Complexes on a Surface. *Angew. Chem., Int. Ed.* **2011**, *50*, 3872–3877.

(9) Cirera, B.; Björk, J.; Otero, R.; Gallego, J. M.; Miranda, R.; Ecija, D. Efficient Lanthanide Catalyzed Debromination and Oligomeric Length-Controlled Ullmann Coupling of Aryl Halides. *J. Phys. Chem. C* **2017**, *121*, 8033–8041.

(10) Bischoff, F.; Seufert, K.; Auwärter, W.; Seitsonen, A. P.; Heim, D.; Barth, J. V. Metalation of Porphyrins by Lanthanide Atoms at Interfaces: Direct Observation and Stimulation of Cerium Coordination to 2H-TPP/Ag(111). *J. Phys. Chem. C* **2018**, *122*, 5083–5092.

DOI: 10.1021/acsnano.8b06704
ACS Nano 2018, 12, 11552–11560

(11) Hellwig, R.; Uphoff, M.; Paintner, T.; Björk, J.; Ruben, M.; Klappenberger, F.; Barth, J. V. Ho-Mediated alkyne reactions at low temperatures on Ag(111). *Chem. - Eur. J.* **2018**, DOI: 10.1002/chem.201803102.
(12) Écija, D.; Urgel, J. I.; Papageorgiou, A. C.; Joshi, S.; Auwärter, W.; Seitsonen, A. P.; Klyatskaya, S.; Ruben, M.; Fischer, S.; Vijayaraghavan, S.; Reichert, J.; Barth, J. V. Five-Vertex Archimedean Surface Tessellation by Lanthanide-Directed Molecular Self-Assembly. *Proc. Natl. Acad. Sci. U. S. A.* **2013**, *110*, 6678−6681.
(13) Urgel, J. I.; Ecija, D.; Auwärter, W.; Barth, J. V. Controlled Manipulation of Gadolinium-Coordinated Supramolecules by Low-Temperature Scanning Tunneling Microscopy. *Nano Lett.* **2014**, *14*, 1369−1373.
(14) Urgel, J. I.; Ecija, D.; Auwärter, W.; Papageorgiou, A. C.; Seitsonen, A. P.; Vijayaraghavan, S.; Joshi, S.; Fischer, S.; Reichert, J.; Barth, J. V. Five-Vertex Lanthanide Coordination on Surfaces: A Route to Sophisticated Nanoarchitectures and Tessellations. *J. Phys. Chem. C* **2014**, *118*, 12908−12915.
(15) Urgel, J. I.; Cirera, B.; Wang, Y.; Auwärter, W.; Otero, R.; Gallego, J. M.; Alcamí, M.; Klyatskaya, S.; Ruben, M.; Martín, F.; Miranda, R.; Ecija, D.; Barth, J. V. Surface-Supported Robust 2d Lanthanide-Carboxylate Coordination Networks. *Small* **2015**, *11*, 6358−6364.
(16) Écija, D.; Urgel, J. I.; Seitsonen, A. P.; Auwärter, W.; Barth, J. V. Lanthanide-Directed Assembly of Interfacial Coordination Architectures−from Complex Networks to Functional Nanosystems. *Acc. Chem. Res.* **2018**, *51*, 365−375.
(17) Ishikawa, N.; Sugita, M.; Ishikawa, T.; Koshihara, S.-Y.; Kaizu, Y. Lanthanide Double-Decker Complexes Functioning As Magnets at the Single-Molecular Level. *J. Am. Chem. Soc.* **2003**, *125*, 8694−8695.
(18) Gatteschi, D.; Sessoli, R.; Villain, J. *Molecular Nanomagnets*; Oxford University, 2006.
(19) Kyatskaya, S.; Galán Mascarós, J. R.; Bogani, L.; Hennrich, F.; Kappes, M.; Wernsdorfer, W.; Ruben, M. Anchoring of Rare-Earth-Based Single-Molecule Magnets on Single-Walled Carbon Nanotubes. *J. Am. Chem. Soc.* **2009**, *131*, 15143−15151.
(20) Rinehart, J. D.; Long, J. R. Exploiting Single-Ion Anisotropy in the Design of f-Element Single-Molecule Magnets. *Chem. Sci.* **2011**, *2*, 2078−2085.
(21) Westerström, R.; Dreiser, J.; Piamonteze, C.; Muntwiler, M.; Weyeneth, S.; Brune, H.; Rusponi, S.; Nolting, F.; Popov, A.; Yang, S.; Dunsch, L.; Greber, T. An Endohedral Single-Molecule Magnet with Long Relaxation Times: Dysc2n@c80. *J. Am. Chem. Soc.* **2012**, *134*, 9840−9843.
(22) Layfield, R. A. Organometallic Single-Molecule Magnets. *Organometallics* **2014**, *33*, 1084−1099.
(23) Liddle, S. T.; van Slageren, J. Improving F-Element Single Molecule Magnets. *Chem. Soc. Rev.* **2015**, *44*, 6655−6669.
(24) Donati, F.; Rusponi, S.; Stepanow, S.; Wäckerlin, C.; Singha, A.; Persichetti, L.; Baltic, R.; Diller, K.; Patthey, F.; Fernandes, E.; Dreiser, J.; Šljivančanin, Ž.; Kummer, K.; Nistor, C.; Gambardella, P.; Brune, H. Magnetic Remanence in Single Atoms. *Science* **2016**, *352*, 318−321.
(25) Natterer, F. D.; Yang, K.; Paul, W.; Willke, P.; Choi, T.; Greber, T.; Heinrich, A. J.; Lutz, C. P. Reading and Writing Single-Atom Magnets. *Nature* **2017**, *543*, 226−228.
(26) Natterer, F. D.; Donati, F.; Patthey, F.; Brune, H. Thermal and Magnetic-Field Stability of Holmium Single-Atom Magnets. *Phys. Rev. Lett.* **2018**, *121*, DOI: 10.1103/PhysRevLett.121.027201.
(27) Franke, K. J.; Schulze, G.; Pascual, J. I. Competition of Superconducting Phenomena and Kondo Screening at the Nanoscale. *Science* **2011**, *332*, 940−944.
(28) Gambardella, P.; Stepanow, S.; Dmitriev, A.; Honolka, J.; de Groot, F. M. F.; Lingenfelder, M.; Gupta, S. S.; Sarma, D. D.; Bencok, P.; Stanescu, S.; Clair, S.; Pons, S.; Lin, N.; Seitsonen, A. P.; Brune, H.; Barth, J. V.; Kern, K. Supramolecular Control of the Magnetic Anisotropy in Two-Dimensional High-Spin Fe Arrays at a Metal Interface. *Nat. Mater.* **2009**, *8*, 189−193.
(29) Barth, J. V. Molecular Architectonic on Metal Surfaces. *Annu. Rev. Phys. Chem.* **2007**, *58*, 375−407.
(30) Barth, J. V. Fresh Perspectives for Surface Coordination Chemistry. *Surf. Sci.* **2009**, *603*, 1533−1541.
(31) Suzuki, T.; Lutz, T.; Payer, D.; Lin, N.; Tait, S. L.; Costantini, G.; Kern, K. Substrate Effect on Supramolecular Self-Assembly: From Semiconductors to Metals. *Phys. Chem. Chem. Phys.* **2009**, *11*, 6498−6504.
(32) Cirera, B.; Đorđević, L.; Otero, R.; Gallego, J. M.; Bonifazi, D.; Miranda, R.; Ecija, D. Dysprosium-Carboxylate Nanomeshes with Tunable Cavity Size and Assembly Motif through Ionic Interactions. *Chem. Commun.* **2016**, *52*, 11227−11230.
(33) Stepanow, S.; Strunskus, T.; Lingenfelder, M.; Dmitriev, A.; Spillmann, H.; Lin, N.; Barth, J. V.; Wóll, C.; Kern, K. Deprotonation-Driven Phase Transformations in Terephthalic Acid Self-Assembly on Cu(100). *J. Phys. Chem. B* **2004**, *108*, 19392−19397.
(34) Wäckerlin, C.; Donati, F.; Singha, A.; Baltic, R.; Rusponi, S.; Diller, K.; Patthey, F.; Pivetta, M.; Lan, Y.; Klyatskaya, S.; Ruben, M.; Brune, H.; Dreiser, J. Giant Hysteresis of Single-Molecule Magnets Adsorbed on a Nonmagnetic Insulator. *Adv. Mater.* **2016**, *28*, 5195−5199.
(35) Dmitriev, A.; Spillmann, H.; Lin, N.; Barth, J. V.; Kern, K. Modular Assembly of Two-Dimensional Metal−organic Coordination Networks at a Metal Surface. *Angew. Chem.* **2003**, *115*, 2774−2777.
(36) Lingenfelder, M. A.; Spillmann, H.; Dmitriev, A.; Stepanow, S.; Lin, N.; Barth, J. V.; Kern, K. Towards Surface-Supported Supramolecular Architectures: Tailored Coordination Assembly of 1,4-Benzenedicarboxylate and Fe on Cu(100). *Chem. - Eur. J.* **2004**, *10*, 1913−1919.
(37) Barth, J. V.; Costantini, G.; Kern, K. Engineering Atomic and Molecular Nanostructures at Surfaces. *Nature* **2005**, *437*, 671.
(38) Payer, D.; Comisso, A.; Dmitriev, A.; Strunskus, T.; Lin, N.; Wöll, C.; DeVita, A.; Barth, J.; Kern, K. Ionic Hydrogen Bonds Controlling Two-dimensional Supramolecular Systems at a Metal Surface. *Chem. - Eur. J.* **2007**, *13*, 3900−3906.
(39) Klappenberger, F.; Arras, E.; Seitsonen, A. P.; Barth, J. V. Nature of the Attractive Interaction between Proton Acceptors and Organic Ring Systems. *Phys. Chem. Chem. Phys.* **2012**, *14*, 15995−16001.
(40) Jeffrey, G. A. *An Introduction to Hydrogen Bonding*; Oxford University Press, 1997.
(41) Cañas-Ventura, M. E.; Klappenberger, F.; Clair, S.; Pons, S.; Kern, K.; Brune, H.; Strunskus, T.; Wöll, C.; Fasel, R.; Barth, J. V. Coexistence of One- and Two-Dimensional Supramolecular Assemblies of Terephthalic Acid on Pd(111) Due to Self-Limiting Deprotonation. *J. Chem. Phys.* **2006**, *125*, 184710.
(42) Clair, S.; Pons, S.; Seitsonen, A. P.; Brune, H.; Kern, K.; Barth, J. V. Stm Study of Terephthalic Acid Self-Assembly on Au(111): Hydrogen-Bonded Sheets on an Inhomogeneous Substrate. *J. Phys. Chem. B* **2004**, *108*, 14585−14590.
(43) Lin, N.; Dmitriev, A.; Weckesser, J.; Barth, J. V.; Kern, K. Real-Time Single-Molecule Imaging of the Formation and Dynamics of Coordination Compounds. *Angew. Chem., Int. Ed.* **2002**, *41*, 4779−4783.
(44) Messina, P.; Dmitriev, A.; Lin, N.; Spillmann, H.; Abel, M.; Barth, J. V.; Kern, K. Direct Observation of Chiral Metal-Organic Complexes Assembled on a Cu(100) Surface. *J. Am. Chem. Soc.* **2002**, *124*, 14000−14001.
(45) Mugarza, A.; Lorente, N.; Ordejón, P.; Krull, C.; Stepanow, S.; Bocquet, M.-L.; Fraxedas, J.; Ceballos, G.; Gambardella, P. Orbital Specific Chirality and Homochiral Self-Assembly of Achiral Molecules Induced by Charge Transfer and Spontaneous Symmetry Breaking. *Phys. Rev. Lett.* **2010**, *105*, DOI: 10.1103/PhysRevLett.105.115702.
(46) Liu, C.; Cohen, J.; Adams, J.; Voter, A. EAM Study of Surface Self-Diffusion of Single Adatoms of Fcc Metals Ni, Cu, Al, Ag, Au, Pd, and Pt. *Surf. Sci.* **1991**, *253*, 334−344.
(47) Clair, S.; Pons, S.; Fabris, S.; Baroni, S.; Brune, H.; Kern, K.; Barth, J. V. Monitoring Two-Dimensional Coordination Reactions:

Directed Assembly of Co−terephthalate Nanosystems on Au(111). *J. Phys. Chem. B* **2006**, *110*, 5627−5632.
(48) Stepanow, S.; Lin, N.; Payer, D.; Schlickum, U.; Klappenberger, F.; Zoppellaro, G.; Ruben, M.; Brune, H.; Barth, J. V.; Kern, K. Surface-Assisted Assembly of 2d Metal−organic Networks That Exhibit Unusual Threefold Coordination Symmetry. *Angew. Chem., Int. Ed.* **2007**, *46*, 710−713.
(49) Hallmark, V. M.; Chiang, S.; Meinhardt, K.-P.; Hafner, K. Observation and Calculation of Internal Structure in Scanning Tunneling Microscopy Images of Related Molecules. *Phys. Rev. Lett.* **1993**, *70*, 3740−3743.
(50) Chiang, S. Scanning Tunneling Microscopy Imaging of Small Adsorbed Molecules on Metal Surfaces in an Ultrahigh Vacuum Environment. *Chem. Rev.* **1997**, *97*, 1083−1096.
(51) Lee, A. F.; Lambert, R. M.; Goldoni, A.; Baraldi, A.; Paolucci, G. On the Coverage-Dependent Adsorption Geometry of Benzene Adsorbed on Pd111: A Study by Fast XPS and NEXAFS. *J. Phys. Chem. B* **2000**, *104*, 11729−11733.
(52) Robledo, M.; Pacchioni, G.; Martín, F.; Alcamí, M.; Díaz-Tendero, S. Adsorption of Benzene on Cu(100) and on Cu(100) Covered with an Ultrathin Nacl Film: Molecule−substrate Interaction and Decoupling. *J. Phys. Chem. C* **2015**, *119*, 4062−4071.
(53) Cotton, S. *Lanthanide and Actinide Chemistry*; John Wiley and Sons, Ldt., 2006.
(54) Seitsonen, A. P.; Lingenfelder, M.; Spillmann, H.; Dmitriev, A.; Stepanow, S.; Lin, N.; Kern, K.; Barth, J. V. Density Functional Theory Analysis of Carboxylate-Bridged Diiron Units in Two-Dimensional Metal−Organic Grids. *J. Am. Chem. Soc.* **2006**, *128*, 5634−5635.
(55) Perdew, J. P.; Burke, K.; Ernzerhof, M. Generalized Gradient Approximation Made Simple. *Phys. Rev. Lett.* **1996**, *77*, 3865−3868.
(56) Blum, V.; Gehrke, R.; Hanke, F.; Havu, P.; Havu, V.; Ren, X.; Reuter, K.; Scheffler, M. Ab Initio Molecular Simulations with Numeric Atom-Centered Orbitals. *Comput. Phys. Commun.* **2009**, *180*, 2175−2196.
(57) Ruiz, V. G.; Liu, W.; Zojer, E.; Scheffler, M.; Tkatchenko, A. Density-Functional Theory with Screened Van Der Waals Interactions for the Modeling of Hybrid Inorganic-Organic Systems. *Phys. Rev. Lett.* **2012**, *108*, 146103.
(58) Krukau, A. V.; Vydrov, O. A.; Izmaylov, A. F.; Scuseria, G. E. Influence of the Exchange Screening Parameter on the Performance of Screened Hybrid Functionals. *J. Chem. Phys.* **2006**, *125*, 224106.
(59) Tersoff, J.; Hamann, D. R. Theory of the Scanning Tunneling Microscope. *Phys. Rev. B: Condens. Matter Mater. Phys.* **1985**, *31*, 805−813.
(60) Shrake, A.; Rupley, J. Environment and Exposure to Solvent of Protein Atoms. Lysozyme and Insulin. *J. Mol. Biol.* **1973**, *79*, 351−371.

DOI: 10.1021/acsnano.8b06704
ACS Nano 2018, 12, 11552−11560

Supporting Information: Assembly of Robust Holmium-Directed 2D Metal-Organic Coordination Complexes and Networks on the Ag(100) Surface

Martin Uphoff,[†,§] Georg S. Michelitsch,[‡,§] Raphael Hellwig,[†] Karsten Reuter,[‡] Harald Brune,[¶] Florian Klappenberger,[*,†] and Johannes V. Barth[*,†]

†*Department of Physics (E20), Technische Universität München, James-Franck-Str. 1, 85748 Garching, Germany*

‡*Department of Chemistry, Chair of Theoretical Chemistry, Technische Universität München, Lichtenbergstr. 4, 85748 Garching, Germany*

¶*Institute of Physics, Ecole Polytechnique Fédérale de Lausanne (EPFL), Station 3, 1015 Lausanne, Switzerland*

§*Contributed equally to this work*

E-mail: florian.klappenberger@tum.de; jvb@tum.de

Organic transition phase

Figure S1(a). shows the organic transition phase, that is formed by deprotonated TPA for low coverages. The phase exhibits a nearly quadratic unit cell of 8.4(1) Å×8.2(2) Å, measured along the slow and fast scanning axis, respectively. The error is calculated from the standard deviation. The islands have no fixed angle in orientation with respect to the lattice and the

distances measured do not show any obvious connection to the lattice vectors. Whilst the difference in the two directions could be drift, it it also likely that the unit cell is indeed not perfectly quadratic. One reason for this is the orientation of the carboxylates, whereby depressions on the edges indicate the deprotonated carboxyl groups (Figure S1(b)). Hence, the molecules are all aligned in the same direction as integral TPA does on metal surfaces[S1]. Since the deprotonated molecule is shorter compared to pristine TPA, it is more difficult to determine if the unit cell is quadratic or rhombohedral. Secondly, the distances between the molecules differ from case to case (even when measured in the same frame). Thirdly, the phase is growing in chains with a width of two to three molecules rather than extended islands. They also can have slight bends. A strictly defined unit cell would not allow this behavior. The fact, that the phase only occurs in these small islands and smoothly connects to the precursor phase (c.f. Figure 1 in the manuscript) indicates it as being a transition phase between single molecules on the surface and extended islands of the precursor phase. Compared to inter-molecular interactions, the molecule-substrate interaction plays a more significant role for the formation of the full monolayer precursor phase, where in every other row the molecules turn by roughly 90° forming the T-facing structure of the precursor phase. Hence, the term transition phase is used.

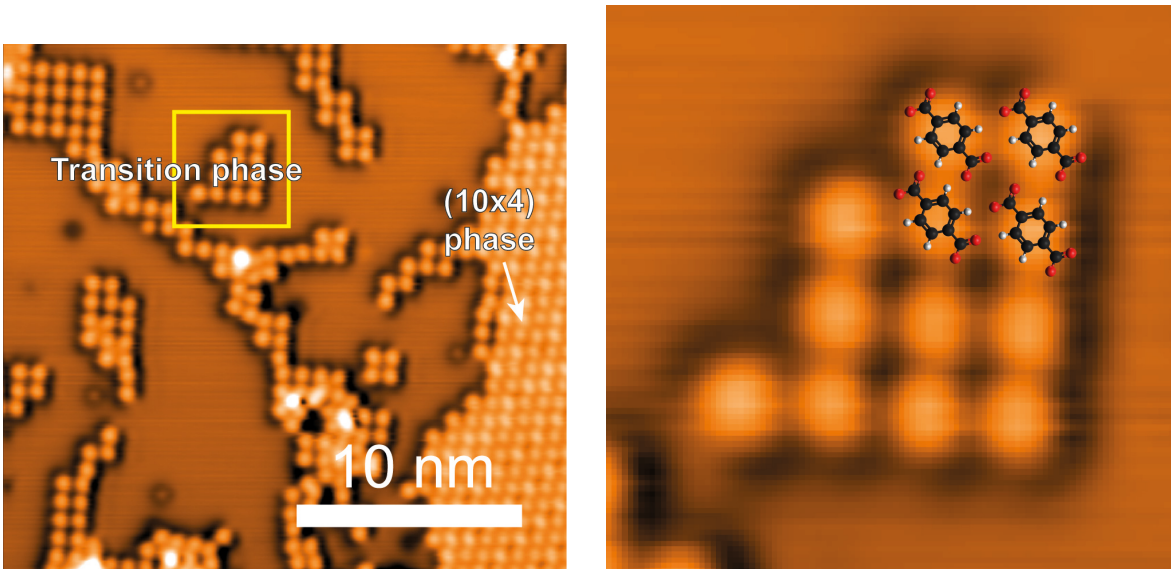

Figure S1: (a) STM image ($I_T = 100\,\mathrm{pA}, V_B = 1\,\mathrm{V}$) of the transition phase (left) next to (10×4) precursor phase (right). The yellow square shows the area enlarged in (b). (b) Enlargement of (a). The depressions on the molecules indicate the position of the carboyxyl groups, revealing a parallel orientation of the molecules.

Chirality of Ho-TPA$_4$ complexes

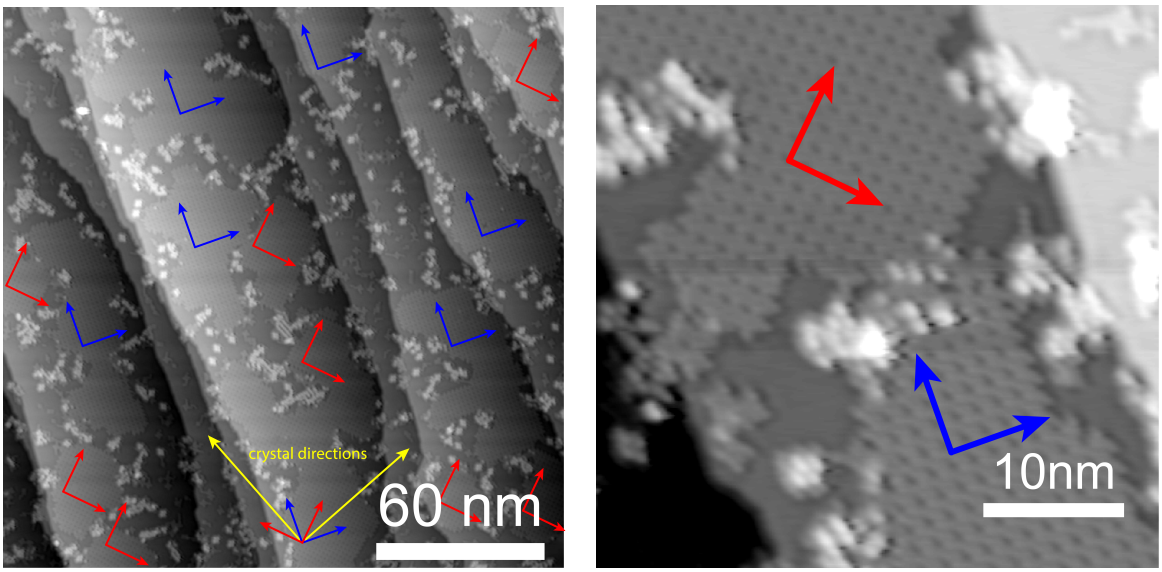

(a) (b)

Figure S2: Constant current STM images showing islands of the cloverleaf phase. There are two directions of growth, indicated by the rectangle arrow pairs in blue or red.

Ho-evaporator

The Ho used in the experiments was evaporated via a foil evaporator. A thin Ho foil (purity= 99.9 %, *Merck*) is heated up by applying a high current, high frequency RF voltage. Due to water cooling of the evaporator, only the foil heats up and emits Ho atoms and clusters of high purity.

Holmium coverage definition

Since Ho is significantly bigger than silver, a full ML of Ho will contain less atoms than a full ML of silver. Additionally, the Ag(100) surface has a quadratic unit cell whilst Ho crystallizes in the hexagonal closed packed structure. This gives a density of 0.652 Ho atoms per silver atom, assuming a full ML. All Ho coverages in this work refer to a full ML of

Ho in the (0001) surface covering the same silver area with a (100) surface. The deposition parameters were calibrated via deposition of Ho on a Ag(111) surface fully covered with Hexakis((trimethylsilyl)ethynyl)benzene (HEB), where Ho adsorbs as single atoms on the phenyl rings of the molecule and are easily countable.

Drift correction

Since STM data has a slow and a fast scan direction, piezo drift will cause a distortion of the images with different magnitudes to each direction. It is essential to overcome this obstacle especially when measuring unit cell sizes of superstructures without having atomic resolution at the same time. A precise calibration of the piezos is obviously essential for corrected length scales of STM data, but the drift effect will nevertheless remain present at all times. A simple and reliable method is to rotate the scan directions by 90° and compare the distorsions. While the calculation of the correction parameters is quite complicated manually, we used the MATLAB script from C. Ophus et al. to calculate the corrected images[S2].

Determination of the U-value

The U-value was determined by optimizing the geometry of $Ho[OAc]_3$ and determining the energetic difference between the occupied and unoccupied *4f* states. Then, the same system was simulated using DFT+U for different values of U and the optimal value determined via a linear fit as shown on the right in Figure S3.

Structural relaxation details

As mentioned in the main manuscript, the checkerboard structure exhibits a large strain as the metal support enforces a cell geometry upon the adsorbate. This is supported by the

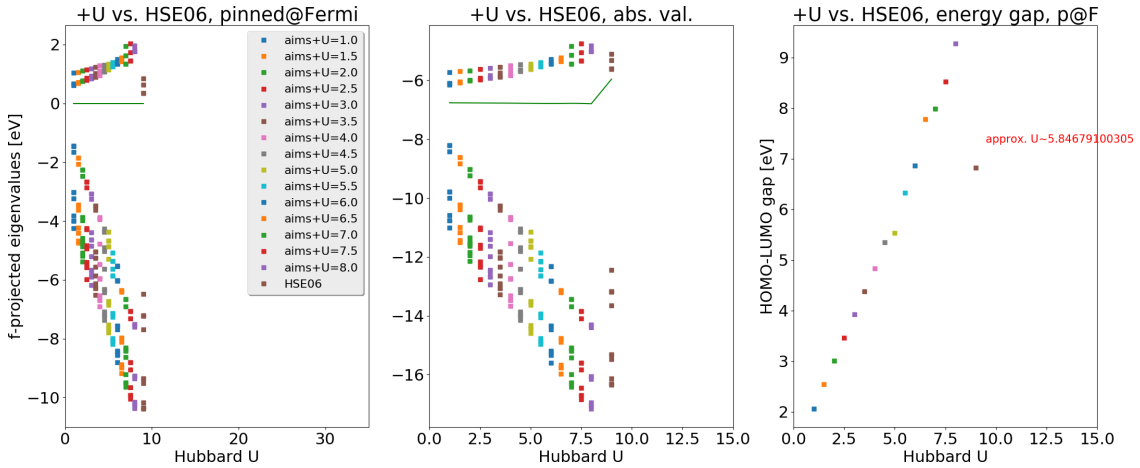

Figure S3: DFT+U screening for a suitable value to reproduce the energetic splitting between the occupied and unoccupied *4f* orbitals in the system. (fltr.: normalized to Fermi-level, absolute values, and the linear fit)

experimental observation of only small islands and stripes of this particular bonding environment. The theoretical modeling of the geometry focused on two different arrangements, where the Ho-atom is located at the hollow (**H1**,**H2**) and bridge (**B**) site, respectively. Relaxation of the first layer of Ag-atoms was permitted. The main features of the experimental STM signature are reproduced by structural models **H2** and **B**. However, the structural model **H2** does not describe a strain-free structure as the largest forces observed exceed 60 meV/Å. Furthermore, although only very small differences are present, the formation energy of structural model **B** is higher than the other two, hinting towards increased thermodynamic stability. The difficulty in assigning a structural model to the *checkerboard* structure supports the experimental observation of the preferred formation of the *cloverleaf* structure instead.

Node bonding environment

The bonding of the carboxylate linkers to the Ho node follows the same motive as already reported for similar Gd-complexes.[S3] Our DFT simulations predict in both observed surface-networks an eight-fold coordination with the carboxylate linker tilted by 52.4 - 53.9° (clover-

STM-simulation & overlay	structure	comments
H1 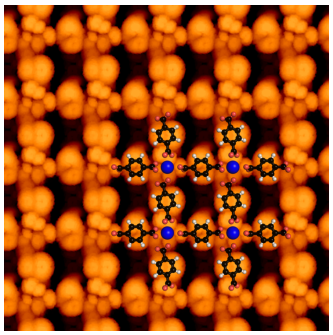	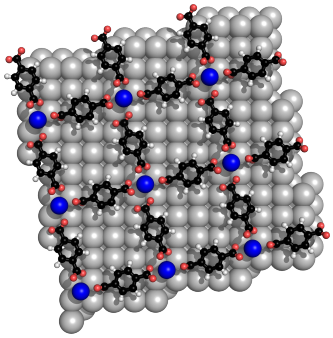	• Ho on hollow-site • $f_{max} < 0.025$ eV/Å • $\Delta E = 147.7$ meV • one TPA is only linked via one O atom to the Ho-atom, which leads to a non-checkerboard pattern observed in the corresponding Tersoff-Haman signatures
H2 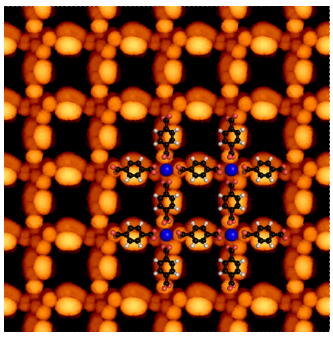	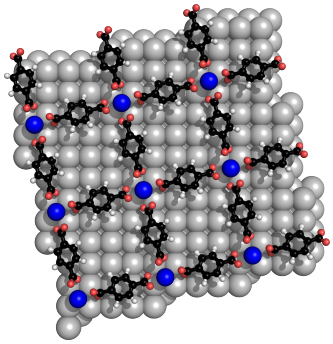	• Ho on hollow-site • $f_{max} <$ **0.060** eV/Å • $\Delta E = 144.3$ meV • In an unstable structure, both TPA molecules would link in a C_4 symmetric fashion to the Ho linker atom. The system shown experiences forces of **60 meV/Å**.
B 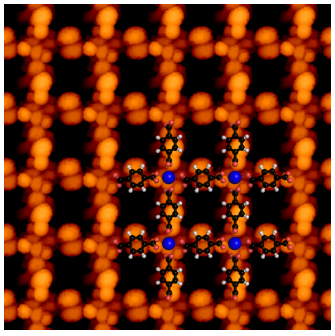	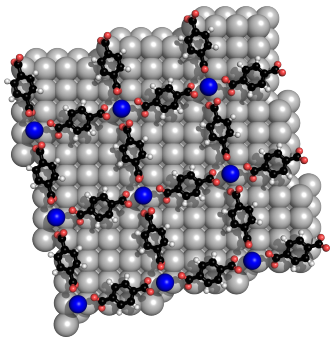	• Ho on bridge-site • $f_{max} < 0.025$ eV/Å • $\Delta E = 147.8$ meV • both TPA molecules are linked in a C_2 symmetric fashion to the Ho linker atom. The system experiences remaining forces up to 25 meV/Å and the STM signatures correspond to the experimental observation.

Figure S4: The different models for the checkerboard structure considered in the DFT simulations.

leaf) and 40.8 - 105° (checkerboard) out-of-plane with respect to the linker backbone. The average bond distance of Ho and O is 2.4Å (cloverleaf) and 2.6Å (checkerboard). A side-view of the bonding environment is given in Figure 5. Also shown in Figure 5 are the forces acting on the individual atoms in the non-equilibrium checkerboard-structure **H2** from Figure S4. The arrows point away from the Ho node, suggesting that an equilibrium would only be reached by detachment from the metal center.

References

(S1) Clair, S.; Pons, S.; Seitsonen, A. P.; Brune, H.; Kern, K.; ; Barth, J. V. Stm Study of Terephthalic Acid Self-Assembly on Au(111): Hydrogen-Bonded Sheets on an Inhomogeneous Substrate. *J. Phys. Chem. B* **2004**, *108*, 14585–14590.

(S2) Ophus, C.; Ciston, J.; Nelson, C. T. Correcting Nonlinear Drift Distortion of Scanning Probe and Scanning Transmission Electron Microscopies from Image Pairs with Orthogonal Scan Directions. *Ultramicroscopy* **2016**, *162*, 1 – 9.

(S3) Urgel, J. I.; Cirera, B.; Wang, Y.; Auwärter, W.; Otero, R.; Gallego, J. M.; Alcamí, M.; Klyatskaya, S.; Ruben, M.; Martín, F.; Miranda, R.; Ecija, D.; Barth, J. V. Surface-Supported Robust 2d Lanthanide-Carboxylate Coordination Networks. *Small* **2015**, *11*, 6358–6364.